



Published in final edited form as:

Bone. 2015 December ; 81: 300–305. doi:10.1016/j.bone.2015.07.033.

Digital Tomosynthesis and High Resolution Computed Tomography as Clinical Tools for Vertebral Endplate Topography Measurements: Comparison with Microcomputed Tomography

Daniel Oravec^a, Abrar Quazi^a, Angela Xiao^a, Ellen Yang^a, Roger Zauel^a, Michael J. Flynn^b, and Yener N. Yeni^{a,*}

^aBone and Joint Center, Henry Ford Hospital, Detroit, MI, United States

^bDepartment of Radiology, Henry Ford Hospital, Detroit, MI, United States

Abstract

Endplate morphology is understood to play an important role in the mechanical behavior of vertebral bone as well as degenerative processes in spinal tissues; however, the utility of clinical imaging modalities in assessment of the vertebral endplate has been limited. The objective of this study was to evaluate the ability of two clinical imaging modalities (digital tomosynthesis, DTS; high resolution computed tomography, HRCT) to assess endplate topography by correlating the measurements to a microcomputed tomography (μ CT) standard. DTS, HRCT, and μ CT images of 117 cadaveric thoracolumbar vertebrae (T10-L1; 23 male, 19 female; ages 36–100 years) were segmented, and inferior and superior endplate surface topographical distribution parameters were calculated. Both DTS and HRCT showed statistically significant correlations with μ CT approaching a moderate level of correlation at the superior endplate for all measured parameters ($R^2_{Adj}=0.19-0.57$), including averages, variability, and higher order statistical moments. Correlation of average depths at the inferior endplate was comparable to the superior case for both DTS and HRCT ($R^2_{Adj}=0.14-0.51$), while correlations became weak or nonsignificant for higher moments of the topography distribution. DTS was able to capture variations in the endplate topography to a slightly better extent than HRCT, and taken together with the higher speed and lower radiation cost of DTS than HRCT, DTS appears preferable for endplate measurements.

Keywords

Vertebral bodies; Endplate topography; Digital tomosynthesis; Microcomputed tomography; Computed tomography

*Corresponding Author. Yener N. Yeni, Ph.D., Bone and Joint Center, Henry Ford Hospital, 2799 West Grand Boulevard, Detroit, Michigan, 48202.

Publisher's Disclaimer: This is a PDF file of an unedited manuscript that has been accepted for publication. As a service to our customers we are providing this early version of the manuscript. The manuscript will undergo copyediting, typesetting, and review of the resulting proof before it is published in its final citable form. Please note that during the production process errors may be discovered which could affect the content, and all legal disclaimers that apply to the journal pertain.

INTRODUCTION

Morphological features of human vertebral body endplates have been shown to be associated with important determinants of bone fragility and degenerative diseases of the spine. For instance, endplate thickness, curvature, and statistical moments of endplate topography distributions have been shown to be associated with vertebral load magnitude and distribution, microstructural properties of the underlying trabecular bone, vertebral failure strain and energy and intervertebral disc degeneration [1–6]. Microcomputed tomography (μ CT) is typically used in such studies to produce a high resolution 3-dimensional depiction of vertebral endplate microarchitecture. However, μ CT is only suitable in a laboratory setting with in vitro specimens due to size limitations and high radiation dose. Measurement of endplate topography using clinically available imaging modalities could improve assessment of vertebral bone quality in a clinical setting. To date, assessment of vertebral endplate using clinical imaging modalities has been limited to measurements such as density, thickness, and gross shape patterns [7–10].

Tomosynthesis was developed as a method to avoid superposition of objects present in conventional radiographic imaging and has evolved since its conception in the 1930s [11] through film [12] and fluoroscopy [13, 14] techniques. Advances in flat panel digital detectors have realized a technology called digital tomosynthesis (DTS) [15]. Digital tomosynthesis is a tomographic imaging modality in which a series of projection images are acquired over a limited arc, with the x-ray source pivoting and translating opposite the direction of a flat panel detector encased in the scanning bed. Musculoskeletal DTS delivers 1/5th the dose or less than that of CT [16–18]. Tomosynthesis reconstructions of the spine are formed in the sagittal or coronal planes, in contrast with CT which produces an axial image with high slice thickness along the superior-inferior direction. Topographic features of the endplate surface are thus captured in-plane with a resolution of approximately 0.24 mm in DTS, rather than the axial resolution of 0.9 mm for HRCT; however, the out of plane slice sensitivity in DTS is about 3 mm [17, 19]. Taken together, these features suggest tomosynthesis might be a preferred clinical imaging modality for geometric analysis of the vertebral endplate.

The current study aims to correlate comparable measures of endplate topography between μ CT, digital tomosynthesis (DTS) and high resolution computed tomography (HRCT) in order to assess the viability of endplate topography measurement in a clinical imaging modality.

METHODS

Human cadaveric thoraco-lumbar spines were acquired under local IRB approval from tissue banks and four vertebral bodies (T10, T11, T12, L1) were harvested from 42 donors. Donors with a history of HIV, hepatitis, diabetes, renal failure, metastatic cancer, osteomalacia, hyperparathyroidism, Paget's disease of bone, spine surgery, cause of death involving trauma, and corticosteroid, anticonvulsant or bisphosphonate use were not included. Vertebral bodies were dissected, soft tissue and posterior elements were removed, and specimens were stored wrapped in saline-soaked gauze at -20° C until scanning was

performed. The donor set consisted of 23 men and 19 women all between the ages of 36 and 100 years. Collectively, the vertebrae of these donors formed a set of 117 bones.

Specimens were mounted and consistently aligned in a custom radiolucent scanning tank filled with 0.9% saline and scanned using DTS (Shimadzu Sonialvision Safire II) and high resolution CT (Siemens Sensation 64). Scanning in saline-filled Lucite tanks (14×14×40 cm) was performed so as to establish bone-water contrast similar to the bone-tissue contrast encountered *in vivo*. Consistent endplate alignment was ensured using a radiolucent clamping system such that the anterior-posterior (AP) and lateral-medial (LM) anatomical directions were aligned to the reconstructed CT image axes. Tomosynthesis scans were performed in two orientations: AP (series of coronal slices) and LM (series of sagittal slices). The same specimens were scanned using a custom-built μ CT system and reconstructed at an isotropic voxel size of 40 micrometers. The μ CT system used in the study was based on the hardware, data acquisition, and reconstruction methods of the μ CT system that has been previously described [20]. The presently operating system uses a Kevex 16-watt x-ray source with a 9-micron focal spot, a 1888×1408-pixel Varian PaxScan 2520 flat panel digital x-ray detector with 127-micron pitch, a Newport precision rotational stage, and control software running under Windows XP.

For HRCT images, a single, unique threshold value in Hounsfield Units was manually determined for each vertebra as the minimum value that delineates bone from soft tissue. The threshold value was used within a custom segmentation algorithm to produce a closed surface grey value mask of the vertebral body [21], from which volume masks separating cortical and cancellous bone were segmented using a previously-described semi-automatic method [22]. The segmentation algorithm consists of dilating the binarized vertebral image twice (closing porosity within and on the surface of the vertebra), applying a median filter (connecting surfaces and smoothing processing artifacts), and eroding back twice. The resulting volume, a solid mask image of the whole vertebral body, was further cropped into separate volumes representing superior and inferior endplates. The topography of each endplate was assessed by creating a 2D height map in which each pixel represented the depth from a fixed plane (the first slice) to the first encounter of bone along the superior-inferior axis using the TopoJ plugin for ImageJ (Figure 1)[23]. The depth distribution (background and holes were eliminated from the analysis) was recorded into a text file in which each row represented a single pixel in 2D height map. The average (AV), standard deviation, skewness (Skew), and kurtosis (Kurt) of the depth measurements were calculated to represent up to the fourth moment of the topography distribution [24]. A high average depth may represent the presence of large surface concavity or many deep pits, while standard deviation of the endplate topography distribution is a measure of endplate surface overall depth variation. Low average and standard deviation of depth are characteristic of a smooth surface. Skewness measures the symmetry of the depth distribution, and may be used as a measure of surface spikiness. Kurtosis measures the spread of the depth distribution (distribution sharpness may be influenced by features such as steep epiphyseal ring or a small number of steep peaks or valleys on the endplate surface). Kurtosis and skewness are understood to affect surface pressure distributions in engineering materials, such that high values of each result in high load bearing ratio and maximum contact pressure

[25]. For instance, the combination of high kurtosis and low skewness has been shown to reduce friction [26].

A similar process was performed for DTS images. A global threshold value was manually determined to delineate bone from soft tissue and air. Due to a blurring effect in the highest and lowest slices of the DTS reconstructions, a central substack of 25 slices (25 mm) was created and the image was binarized in ImageJ using the recorded threshold value (Figure 2a). Binarized images were cropped into separate volumes representing superior and inferior endplates. Depth distributions were again calculated for DTS endplate images and distribution statistics were calculated from DTS depth measurements. Additionally, depth frequencies were concatenated prior to calculating distribution statistics in order to create a pooled variable, representing a composite of the two DTS scanning directions.

Threshold values for μ CT reconstructions were calculated from a $300 \times 300 \times 300$ voxel central cube of cancellous bone using the Otsu method in ImageJ and the whole image was binarized using this global threshold value. A custom algorithm was used to produce a depth frequency distribution representing distances from the superior-most and inferior-most reference planes to the inner surfaces of the vertebral endplate [6]. The custom algorithm used an approach similar to that of TopoJ but additional procedures were used to account for small voids present on the vertebral endplate in high resolution μ CT images. In this method, surface voxels were compared to the surrounding neighborhood of voxels such that if a surface voxel is deeper than the mean plus 0.5 standard deviation of its neighborhood, the surface voxel was considered to be part of an open hole. Interpolating depths for open holes as the reciprocal-distance-squared weighted average of the neighborhood ensured a contiguous endplate surface. Distribution statistics were again calculated using the depth frequency distribution produced by this method for μ CT.

For statistical analyses, the main interest was in the relationship between similar measurements from the μ CT and DTS images and between those from the μ CT and high resolution CT (HRCT) images. The relationships between μ CT and DTS/HRCT variables were examined using mixed regression models with μ CT variable as the outcome and the corresponding DTS or HRCT variable as the effect variable. The model included a random subject variable to account for pseudoreplication due to using multiple vertebral levels from some subjects. In order to gain further insight into the nature of examined relationships, differences in mean of statistical distribution parameters between superior and inferior endplates were examined for μ CT images using paired t-tests. All analyses were performed in JMP (Version 7.0, SAS Institute Inc., Cary, NC).

In an effort to understand the feasibility of endplate topography measurements in clinical DTS images, two vertebral levels (T12, L1) were assessed from a single *in vivo* thoracolumbar spine DTS image using the same methods presented above for comparison with average outcome measures from the 117 *in vitro* specimens (Figure 4). DTS scans of the patient (87Y male) were performed under IRB approval in the context of a metabolic survey for multiple myeloma.

RESULTS

For the superior endplate, except for kurtosis calculated from pooled AP and LM DTS images, all DTS and HRCT measurements were significantly associated with the corresponding μ CT measurements (Table 1). Calculations from μ CT had stronger associations with those from AP DTS than with LM DTS for μ CT.Av and μ CT.SD but not for higher order moments, as indicated by R^2_{Adj} values. Pooling the AP and LM images before calculation or averaging the results from the AP and LM views did not improve R^2_{Adj} values.

For the inferior endplate, all DTS and HRCT based average measurements were associated with μ CT.Av (Table 2). SD measured from μ CT (μ CT.SD) was associated with SD measured from LM DTS but not from AP DTS. No significant relationship was found for higher order moments of the topography distribution for the inferior endplate. The relationship between μ CT and HRCT was statistically significant for skewness; however, the slope of the regression was negative, indicating a superfluous relationship. In contrast with results for the superior endplate, calculations from μ CT had stronger associations with those from LM DTS than with AP DTS. Pooling the AP and LM images before calculation or averaging the results from the AP and LM views did not improve R^2_{Adj} values.

HRCT was generally comparable to or slightly better than DTS in predicting average depth measurements and third and fourth order moments of the depth distribution but was outperformed by DTS in predicting SD of the distributions (Tables 1 and 2). The slopes of the relationships were closer to 1 (ideal relationship) for DTS than for HRCT indicating a lack of accuracy for HRCT. In addition, average and standard deviation of depth distributions were generally closer to that of μ CT than were higher order statistical parameters.

Paired t-test results indicated that the mean values of average, standard deviation, and kurtosis of endplate topography distributions measured from μ CT images are significantly different between superior and inferior endplates (Table 3). Average and Kurtosis were significantly higher at the superior endplate, while standard deviation was lower.

All measured parameters from *in vivo* DTS vertebral images were within the range of *in vitro* data (Table 4).

DISCUSSION

To our knowledge, this is the first study to demonstrate the ability to measure voxel-based topography of the entire vertebral endplate surface using clinical imaging modalities. Both tested modalities showed statistically significant correlations with μ CT approaching a moderate level of correlation at the superior endplate for all measured parameters ($R^2_{Adj}=0.19-0.57$, Figure 3), including averages, variability, and higher order statistical moments. Correlation of average depths at the inferior endplate was comparable to the superior case for both DTS and HRCT ($R^2_{Adj}=0.14-0.51$), while correlations became weak or nonsignificant for higher moments of the topography distribution.

DTS and HRCT have distinct advantages over each other that may help explain slightly better performance of one over the other for different measurements. Due to the blurring of the lowest and highest slices, the most lateral regions of the vertebra are excluded from analysis in the LM view, and the most anterior and posterior regions are excluded from analysis in the AP view for DTS scans (Figure 2a). In addition, DTS has a large slice thickness (1 mm), resulting in low out of plane resolution for a given plane of view. Due to these features, DTS has poorer sampling of some regions on the endplate surface (Figure 2b). Therefore, a slightly better performance of HRCT in measurement of average depths may be due to its sampling from a more complete space than does DTS in the axial plane. On the other hand, DTS has considerably higher resolution than HRCT in the planes of measurement (sagittal plane in LM and coronal plane in the AP scans), providing better precision for the depth values measured (Figure 2c). Such precision would help characterize the variations the depth distributions more accurately. This may explain the correlations of SD values between DTS and μ CT for the inferior endplate where the measured distances are small.

Weaker correlations in higher order distribution statistics (Tables 1–2) for both DTS and HRCT at the inferior endplate are consistent with paired t-test results which indicated that average depth from the reference plane was significantly greater at the superior endplate (Table 3). These findings are supported by *in vivo* radiographic endplate morphology studies which indicate that the inferior endplate is typically flatter with less concavity depth than the superior endplate [9]. Provided that DTS and HRCT have approximately 7–17 times lower measurement resolution than μ CT, ability to measure differences within the topography distribution will be potentially largely affected by average depth. With a greater average depth, there are more steps available at a given voxel size to define the characteristic features contributing to changes in higher order statistical parameters.

At the superior endplate, skewness had higher correlations with μ CT than kurtosis for both DTS and HRCT (Table 1). This apparent trend may be explained such that skewness, a measure of distribution asymmetry, is less sensitive to quantization of the sampling space resulting from low resolution than kurtosis, which is highly sensitive to outliers in the depth distribution (features such as high peaks in endplate morphology). Such outlying features may be missed due to infrequent sampling in coronal/sagittal directions, largely affecting kurtosis calculations. Additionally, HRCT had slightly better correlations than DTS for both skewness and kurtosis, which suggests this trend is due to pixel spacing in coronal/sagittal planes and not due to axial pixel spacing, provided that resolution in the measurement direction is considerably less in HRCT than DTS (Figure 2).

The current findings indicate that the topography of the endplate surface is different between the superior and inferior endplates of the same vertebra. In addition to differences in depth, we found that coronal planes (AP view, in which the endplate would be sampled with higher resolution in the transverse direction) provide more information on the superior endplate whereas sagittal planes (LM view, in which the endplate would be sampled with higher resolution in the anteroposterior direction) provide more information on the inferior endplates. This finding suggests that the nonuniformity of endplate surface is aligned in different directions for the superior endplate than for the inferior endplate. While the reasons

for this may be subject of future research, this result indicates that both endplates of a vertebra should be evaluated separately during imaging studies.

Several limitations of the present study have been noted. Manual selection of threshold values produced visually acceptable segmentation (Figure 1b–c), however methods may be refined to use image pre-processing and adaptive thresholding techniques in order to optimize and standardize characterization of the endplate surface. In addition, aside from error attributed to differences in resolution between DTS/CT and μ CT, shadow artifacts inherent to limited angle tomography (objects remaining visible in slices remote to their focus plane) may contribute to error between the DTS and μ CT. Although posterior elements were removed to facilitate μ CT scanning in this *in vitro* experiment, artifacts resulting from the presence of posterior elements have a minimal impact on adjacent reconstructed layers in clinical DTS scans. Preliminary data suggests that clinical DTS scans can be effectively thresholded and processed for endplate topography measurements (Figure 4).

Although analysis of topography from statistical distributions allows general characterization of endplate surface attributes such as average depth, depth variability and presence of extreme features such as spikes and valleys, methods assessing spatial distribution and size scale of topography should be explored. As mentioned, higher order statistics are especially prone to artifacts from voids and edges. Therefore, care was taken to prepare analysis regions so as to avoid, for example, high remnants from posterior elements and improper delineation of endplate vs. cortical shell at the vertebral rim. In clinical studies, posterior elements should be similarly avoided when defining endplate analysis regions. Development of a practical, semi-automated algorithm for endplate segmentation and topography measurement in future effort could help translation to clinical assessment of vertebral endplate.

While the current study suggests that DTS can be used for characterization of endplates *in vitro*, the feasibility of translation to assessment of *in vivo* DTS images is unknown. As previously discussed, it is not possible to use microcomputed tomography as a gold standard for comparison with clinical images. The preliminary evidence that *in vivo* DTS images can be processed to segment vertebral endplate using the same protocols as *in vitro* specimens, together with relative agreement of the calculated values (Table 4), suggests that *in vivo* endplate topography measurement is feasible. Although the accuracy of the measured variables needs further improvement, the relationships found in the current study might be useful on a comparative basis.

In conclusion, DTS and HRCT performed comparably for measurement of average distances, both having moderate levels of correlations with μ CT. DTS was able to capture variations in the endplate topography to a slightly better extent than HRCT. Based on these findings and the higher speed and lower radiation cost of DTS than HRCT, DTS appears preferable for endplate measurements. It remains to be seen the extent to which DTS based assessment of endplate geometry will help elucidate the degenerative processes underlying the degradation of spinal tissue qualities in a clinical setting.

ACKNOWLEDGEMENTS

This project was supported, in part, by the National Institutes of Health under Grant Number AR059329. Its contents are solely the responsibility of the authors and do not necessarily represent the official views of the NIH. David Hovis, Ph.D. of Case Western Reserve University Swagelok Center for Surface Analysis of Materials provided a modified version of the TopoJ plugin for ImageJ. Human tissue used in the presented work was provided by NDRI (National Disease Research Interchange) and Platinum Training.

REFERENCES

1. Eswaran SK, Gupta A, Keaveny TM. Locations of bone tissue at high risk of initial failure during compressive loading of the human vertebral body. *Bone*. 2007; 41:733–739. [PubMed: 17643362]
2. Hulme PA, Boyd SK, Ferguson SJ. Regional variation in vertebral bone morphology and its contribution to vertebral fracture strength. *Bone*. 2007; 41:946–957. [PubMed: 17913613]
3. Langrana NA, Kale SP, Edwards WT, Lee CK, Kopacz KJ. Measurement and analyses of the effects of adjacent end plate curvatures on vertebral stresses. *Spine J*. 2006; 6:267–278. [PubMed: 16651220]
4. Pappou IP, Cammisa FP, Girardi FP. Correlation of end plate shape on MRI and disc degeneration in surgically treated patients with degenerative disc disease and herniated nucleus pulposus. *Spine Journal*. 2007; 7:32–38. [PubMed: 17197330]
5. Roberts S, McCall IW, Menage J, Haddaway MJ, Eisenstein SM. Does the thickness of the vertebral subchondral bone reflect the composition of the intervertebral disc? *Eur Spine J*. 1997; 6:385–389. [PubMed: 9455665]
6. Nekkanty S, Yerramshetty J, Kim DG, Zael R, Johnson E, Cody DD, Yeni YN. Stiffness of the endplate boundary layer and endplate surface topography are associated with brittleness of human whole vertebral bodies. *Bone*. 2010; 47:783–789. [PubMed: 20633709]
7. Noshchenko A, Plaseied A, Patel VV, Burger E, Baldini T, Yun L. Correlation of Vertebral Strength Topography With 3-Dimensional Computed Tomographic Structure. *Spine*. 2013; 38:339–349. [PubMed: 22869060]
8. Lakshmanan P, Purushothaman B, Dvorak V, Schrott W, Thambiraj S, Boszczyk M. Sagittal endplate morphology of the lower lumbar spine. *Eur Spine J*. 2012; 21(Suppl 2):S160–S164. [PubMed: 22315035]
9. Wang Y, Battie MC, Videman T. A morphological study of lumbar vertebral endplates: radiographic, visual and digital measurements. *Eur Spine J*. 2012; 21:2316–2323. [PubMed: 22743647]
10. van der Houwen EB, Baron P, Veldhuizen AG, Burgerhof JG, van Ooijen PM, Verkerke GJ. Geometry of the intervertebral volume and vertebral endplates of the human spine. *Ann Biomed Eng*. 2010; 38:33–40. [PubMed: 19876738]
11. Ziedses des Plantes BG. Seriescopy, Een Rontgenographische method welke het mogelijk maakt achtereenvolgens een oneindig aantal evenwijdige vlakken van het te onderzoeken voorwerp afzonderlijk te bechouwen (Seriescopy, a Roentgenographic method which allows an infinite number of successive parallel planes of the test object to be considered separately) (English translation). *Ned Tijdschr Geneesk*. 1935; 51:5852–5856.
12. Garrison JB, Grant DG, Guier WH, Johns RJ. Three dimensional roentgenography. *Am J Roentgenol Radium Ther Nucl Med*. 1969; 105:903–908.
13. Hoefler EE, Grimmert H, Kieslich B. Computer-controlled synthesis of tomograms by means of a TV storage tube. *IEEE Trans Biomed Eng*. 1974; 21:243–244. [PubMed: 4851134]
14. Lasser EC, Baily NA, Crepeau RL. A fluoroplanigraphy system for rapid presentation of single plane body sections. *Am J Roentgenol Radium Ther Nucl Med*. 1971; 113:574–577.
15. Godfrey DJ, Rader A, Dobbins Iii JT. Practical strategies for the clinical implementation of matrix inversion tomosynthesis (MITS). 2003:379–390.
16. Gazaille RE 3rd, Flynn MJ, Page W 3rd, Finley S, van Holsbeeck M. Technical innovation: digital tomosynthesis of the hip following intra-articular administration of contrast. *Skeletal Radiol*. 2011; 40:1467–1471. [PubMed: 21822939]

17. Flynn, MJ.; McGee, R.; Blechinger, J. Spatial resolution of x-ray tomosynthesis in relation to computed tomography for coronal/sagittal images of the knee; 2007 Spie Conference, Medical Imaging; San Diego, CA. 2007.
18. Zhang, Y.; Xiang, L.; Segars, WP.; Samei, E. Comparative dosimetry of radiography, tomosynthesis, and CT for chest imaging across 59 adult patients; 2013 Spie Conference, Medical Imaging; Lake Buena Vista, FL. 2013.
19. Thornton, MM.; Flynn, MJ. Measurement of the spatial resolution of a clinical volumetric computed tomography scanner using a sphere phantom; 2006 SPIE Conference, Medical Imaging; San Diego, CA. 2006. p. 61421Z61421Z-61421Z-10.
20. Reimann DA, Hames SM, Flynn MJ, Fyhrie DP. A cone beam computed tomography system for true 3D imaging of specimens. *Appl Radiat Isot.* 1997; 48:1433–1436. [PubMed: 9463869]
21. Zael, R.; Fyhrie, DP.; Yeni, YN. Segmentation Algorithm With Improved Connectivity For Accurate 3D Representation Of Microcomputed Tomographic Images Of Human Vertebral Bodies; 51st Annual Meeting of the Orthopaedic Research Society; Washington, D.C.. 2005. p. 1260
22. Buie HR, Campbell GM, Klinck RJ, MacNeil JA, Boyd SK. Automatic segmentation of cortical and trabecular compartments based on a dual threshold technique for in vivo micro-CT bone analysis. *Bone.* 2007; 41:505–515. [PubMed: 17693147]
23. Rasband, WS. ImageJ. U.S. National Institutes of Health; 1997–2014.
24. ASME. Surface texture : surface roughness, waviness and lay. New York: American Society of Mechanical Engineers; 2003.
25. Wang WZ, Chen H, Hu YZ, Wang H. Effect of surface roughness parameters on mixed lubrication characteristics. *Tribology International.* 2006; 39:522–527.
26. Sedlacek M, Vilhena LMS, Podgornik B, Vizintin J. Surface Topography Modelling for Reduced Friction. *Strojnicki Vestnik-Journal of Mechanical Engineering.* 2011; 57:674–680.

Highlights

We evaluated DTS and HRCT vs. micro-CT for measurement of endplate topography.

Moderate levels of correlation found between both DTS and HRCT vs. micro-CT.

DTS captured variations in endplate topography slightly better than CT.

DTS appears to be preferable for measurement of endplate topography.

This is the first use of DTS in measurement of endplate topography.

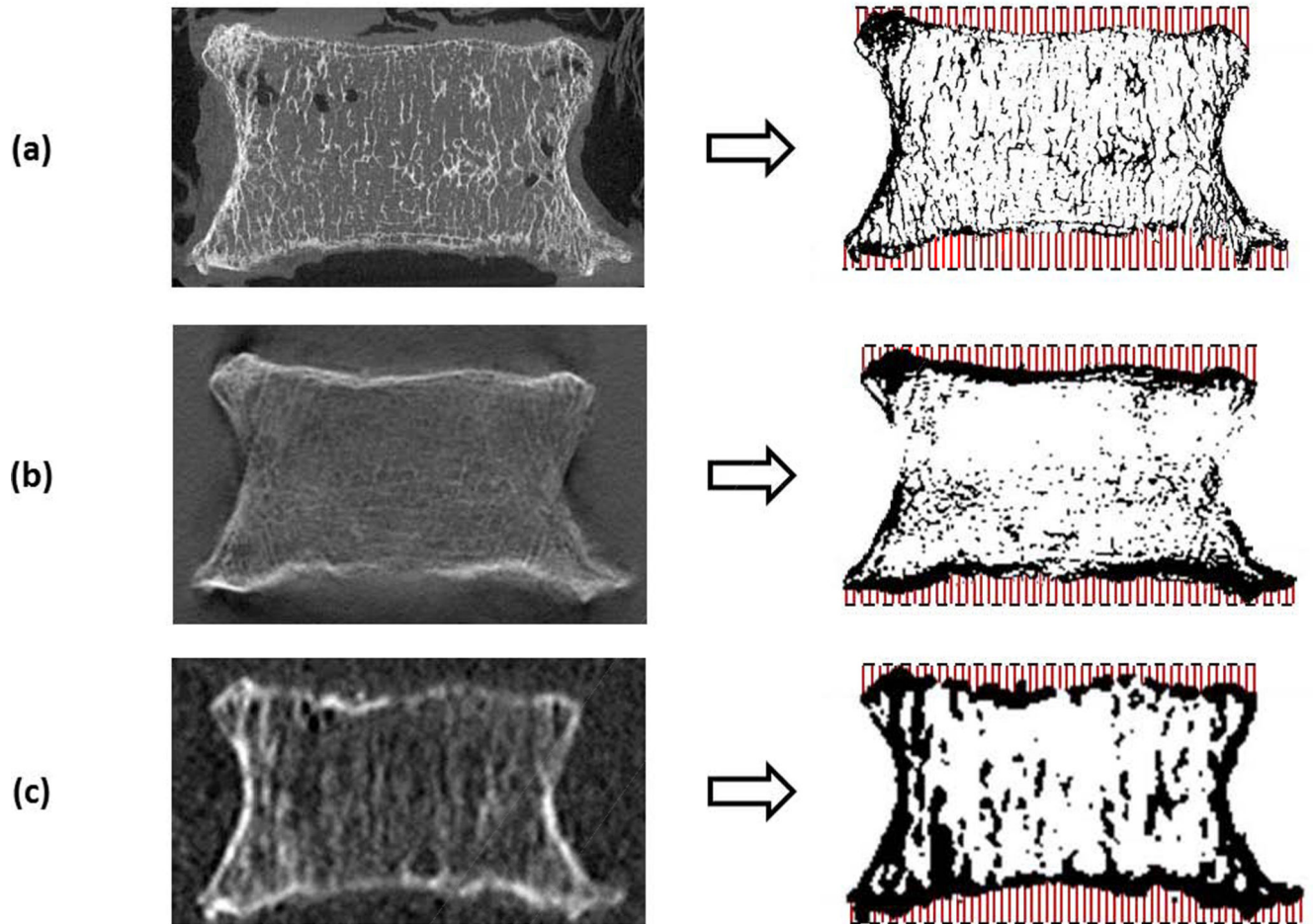


Figure 1.

Images were thresholded and depth distributions calculated from a fixed plane (dashed lines) at the superior and inferior endplates. Comparison of images taken from sagittal plane in similar regions from (a) μ CT, (b) DTS (AP), and (c) HRCT. Images are resized to show detail at comparable scale.

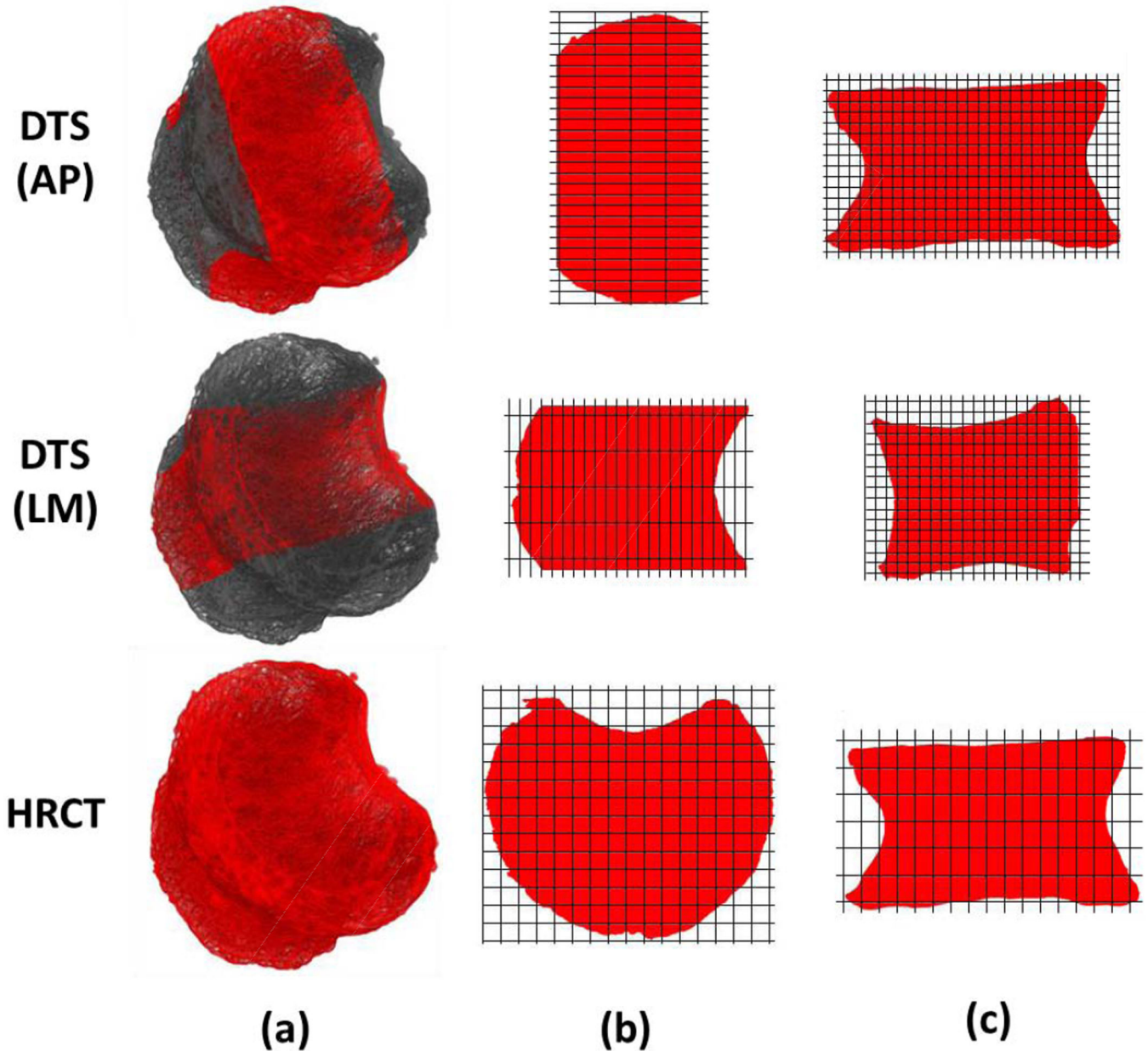


Figure 2.

(a) The analysis volume was prescribed as a 25 mm central slab in AP and LM DTS images to avoid blurring artifact, while HRCT VOI included the entire volume. Thus, the entire endplate was sampled for HRCT while a portion of the endplate was used in the DTS analysis. The portion of the endplate included in the DTS analysis depended on the view. (b) Note that pixel size is anisotropic in axial DTS images while it is isotropic in axial HRCT images. Within the volume included in the analysis, the quantity and spacing of sample points available for analysis is better in sagittal planes but poorer in coronal planes for AP DTS than for HRCT. In contrast, the quantity and spacing of sample points available for analysis is better in coronal planes but poorer in sagittal planes for LM DTS than for HRCT. (c) Pixel size is anisotropic in the measurement plane for HRCT images (with measurement

resolution corresponding to slice thickness) and isotropic (coronal for AP, sagittal for LM) for DTS. DTS has superior sampling resolution along the axes perpendicular/parallel to the scanning direction, providing DTS considerably higher measurement resolution than HRCT within each plane of analysis. Note that grid lines demonstrate relative pixel spacing in DTS vs. HRCT and are not drawn to scale; figure prepared from μ CT images for clarity.

Author Manuscript

Author Manuscript

Author Manuscript

Author Manuscript

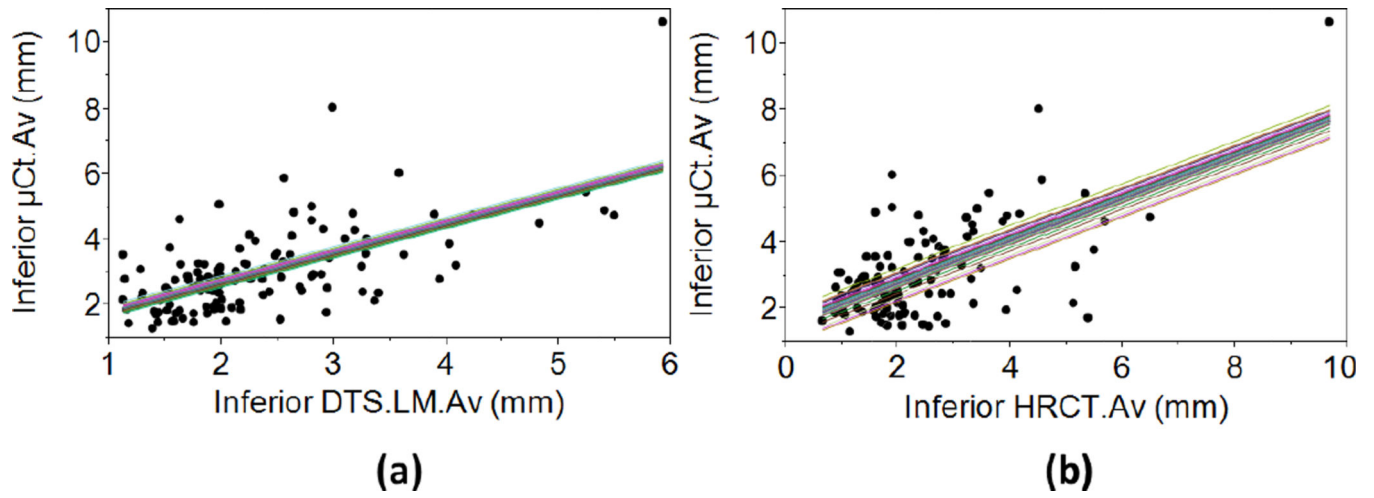


Figure 3. Mixed regression plots of (a) inferior DTS.LM.Av vs. $\mu\text{CT.Av}$, $R^2_{\text{Adj}}=0.47$ and (b) inferior HRCT.Av vs. $\mu\text{CT.Av}$, $R^2_{\text{Adj}}=0.51$. The closeness of individual regression lines indicates that the effect of donor on the regression equation is small.

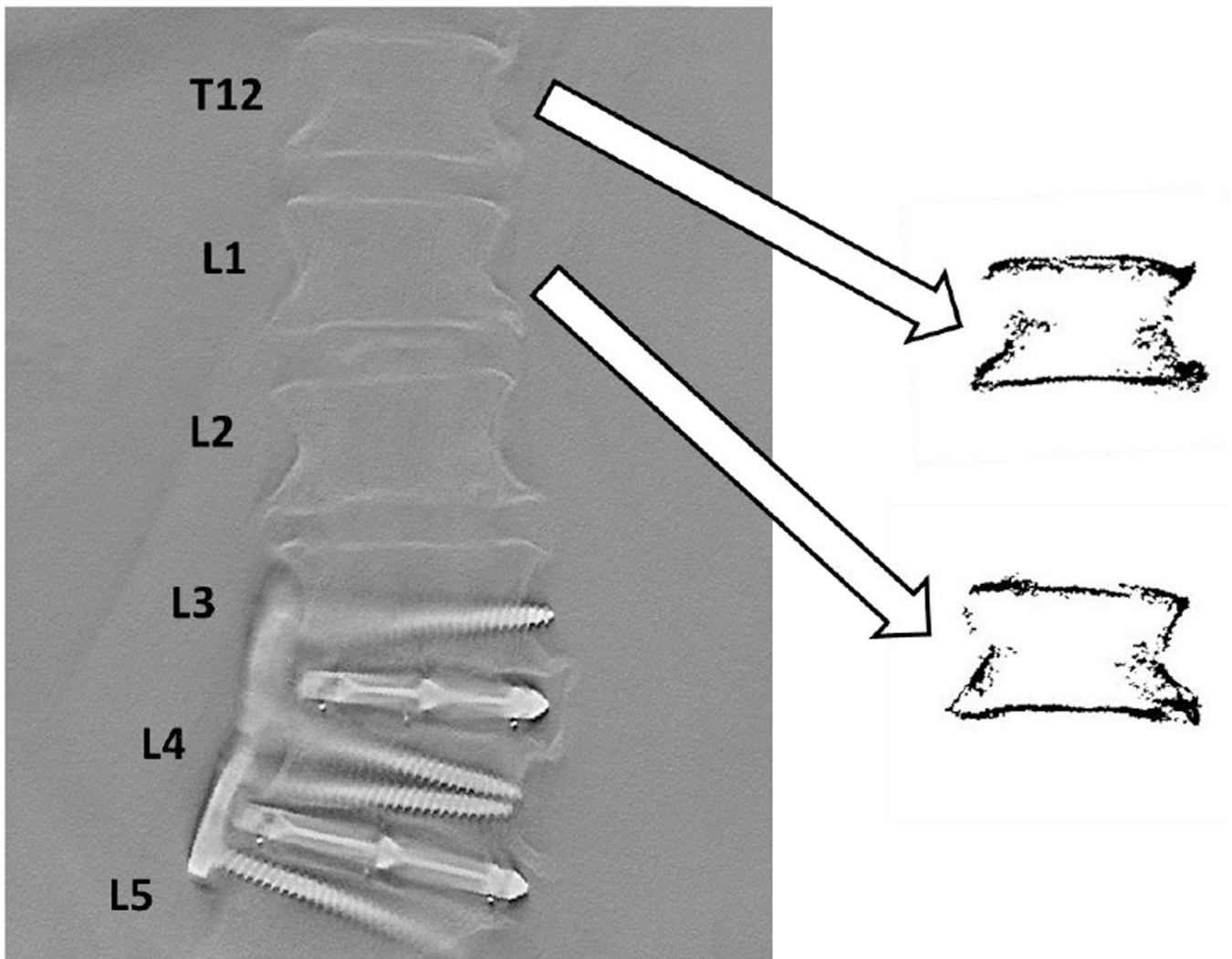


Figure 4. Endplate topography measurements were successfully performed on two vertebral levels (T12, L1) from the same patient using clinical DTS images. Vertebral levels were selected so as to match *in vitro* levels and avoid implants at L3–L5. Images of T12 and L1 vertebrae were separated and thresholded (right) and depth distributions calculated using the same methods described for *in vitro* specimens. Measured parameters were well within the range of *in vitro* specimens (Table 4).

Results from mixed models comparing μ CT to DTS and HRCT topography measurements at superior endplates. The symbol \cup indicates that the depth measurements from AP and LM views were pooled before calculation of the distribution statistics. The symbol \cup indicates that the distribution statistics from AP and LM views were averaged. For ease of comparison with DTS/HRCT averages, μ CT averages are presented below each parameter in parentheses.

Table 1

	μ CT,Av (Av=3.83)	μ CT,SD (Av=1.21)	μ CT,Sk (Av=-0.60)	μ CT,Ku (Av=3.43)
DTS,AP				
Av	2.63	0.97	-0.08	0.51
R ² _{Adj}	0.34	0.32	0.52	0.31
Slope	0.612	0.747	0.179	0.246
P _d	<0.0001	<0.0001	<0.03	<0.004
Intercept	2.214	0.476	-0.576	3.293
P _{int}	<0.0001	<0.002	<0.0001	<0.0001
DTS,LM				
Av	2.79	0.95	-0.47	0.17
R ² _{Adj}	0.21	0.27	0.51	0.31
Slope	0.629	0.876	0.392	0.239
P _d	<0.0001	<0.0001	<0.0001	<0.002
Intercept	2.048	0.366	-0.396	3.336
P _{int}	<0.0001	<0.002	<0.0001	<0.0001
DTS,APULM				
Av	2.71	1.05	-0.11	0.06
R ² _{Adj}	0.30	0.20	0.53	
Slope	0.829	0.675	0.362	
P _d	<0.0001	<0.0001	<0.0005	NS
Intercept	1.565	0.486	-0.553	
P _{int}	<0.0001	<0.0004	<0.0001	
DTS,AP LM				
Av	2.71	0.96	-0.28	0.34
R ² _{Adj}	0.30	0.31	0.50	0.30
Slope	0.815	0.929	0.441	0.422
P _d	<0.0001	<0.0001	<0.0001	<0.0001

	$\mu_{CT,AV}$ (AV=3.83)	$\mu_{CT,SD}$ (AV=1.21)	$\mu_{CT,Sk}$ (AV=-0.60)	$\mu_{CT,Ku}$ (AV=3.43)
Intercept	1.601	0.309	-0.465	3.252
P_{int}	<0.0001	<0.02	<0.0001	<0.0001
<hr/>				
AV	2.89	0.88	-0.83	1.00
R²_{Adj}	0.37	0.19	0.57	0.40
Slope	0.443	0.550	0.256	0.234
P_{sl}	<0.0001	<0.0001	<0.004	<0.0009
Intercept	2.555	0.717	-0.373	3.151
P_{int}	<0.0001	<0.0001	<0.0003	<0.0001

Results from mixed models comparing μ CT to DTS and HRCT topography measurements at inferior endplates. The symbol \cup indicates that the depth measurements from AP and LM views were pooled before calculation of the distribution statistics. The symbol \cup indicates that the distribution statistics from AP and LM views were averaged. For ease of comparison with DTS/HRCT averages, μ CT averages are presented below each parameter in parentheses.

Table 2

	μ CT,Av (Av=2.96)	μ CT,SD (Av=1.89)	μ CT,Sk (Av=-0.66)	μ CT,Ku (Av=2.23)
DTS,AP				
Av	2.18	0.88	0.18	0.68
R ² _{Adj}	0.14			
Slope	0.651			
P _d	<0.0001	NS	NS	NS
Intercept	1.624			
P _{int}	<0.0001			
DTS,LM				
Av	2.32	0.93	-0.15	0.15
R ² _{Adj}	0.47	0.30		
Slope	0.892	0.546		
P _d	<0.0001	<0.03	NS	NS
Intercept	0.921	1.410		
P _{int}	<0.0004	<0.0001		
DTS,APULM				
Av	2.24	0.99	0.18	0.31
R ² _{Adj}	0.32	0.35		
Slope	1.112	0.925		
P _d	<0.0001	<0.0001	NS	NS
Intercept	0.525	0.986		
P _{int}	>0.09	<0.0002		
DTS,AP LM				
Av	2.25	0.90	0.01	0.41
R ² _{Adj}	0.34	0.28		
Slope	1.120	0.611		
P _d	<0.0001	<0.04	NS	NS

	$\mu_{CT,Av}$ ($AV=2.96$)	$\mu_{CT,SD}$ ($AV=1.89$)	$\mu_{CT,Sk}$ ($AV=-0.66$)	$\mu_{CT,Ku}$ ($AV=2.23$)
Intercept	0.496	1.366		
P_{int}	>0.10	<0.0001		
<hr/>				
AV	2.35	0.73	-0.54	1.13
R²_{Adj}	0.51		0.23	
Slope	0.636		-0.273	
P_{sl}	<0.0001	NS	<0.02	NS
Intercept	1.502		-0.789	
P_{int}	<0.0001		<0.0001	

Table 3

Paired t-test results comparing statistical distribution parameters between superior and inferior endplates in μ CT images. Average parameters for superior and inferior endplate are presented as \pm standard deviation.

Parameter	p-value	Superior Endplate	Inferior Endplate
AV (mm)	<0.0001	3.832 \pm 1.367	2.956 \pm 1.148
SD (mm)	<0.0001	1.205 \pm 0.523	1.891 \pm 0.908
Skew	0.4358	-0.598 \pm 0.589	-0.664 \pm 1.022
Kurt	<0.0001	3.428 \pm 1.288	2.226 \pm 0.898

Preliminary comparison between endplate topography measurements made from *in vivo* and *in vitro* vertebral body images. For *in vivo* measurements, distribution parameters are presented for two vertebral levels from the same patient (supine/AP scan, T12, L1). Average distribution parameters are presented for 117 *in vitro* specimens followed by range (Min, Max). All *in vivo* measurements were within the range of the *in vitro* cohort.

Table 4

	Scan type	Parameter	Av (mm)	SD (mm)	Kurt	Skew
Superior	<i>in vivo</i>	T12, L1	2.53, 4.10	0.94, 1.07	0.82, 0.10	0.84, -0.16
	<i>in vitro</i>	T10-L1 AP Av (Min, Max)	2.64 (0.96, 5.57)	0.97 (0.50, 2.09)	0.49 (-1.18, 8.24)	-0.09 (-1.02, 2.33)
Inferior	<i>in vivo</i>	T12, L1	4.10, 3.80	0.87, 0.83	1.05, 0.02	-0.92, -0.61
	<i>in vitro</i>	T10-L1 AP Av (Min, Max)	2.18 (0.64, 5.12)	0.87 (0.44, 2.51)	0.67 (-1.20, 13.06)	0.17 (-1.79, 2.73)